Acta Neuropathologica (2019) 138:613–630
https://doi.org/10.1007/s00401-019-02048-2

ORIGINAL PAPER

Impact of TREM2 risk variants on brain region-specific immune activation and plaque microenvironment in Alzheimer's disease patient brain samples

Stefan Prokop[1,2,3,4] · Kelly R. Miller[1,5] · Sergio R. Labra[1] · Rose M. Pitkin[1] · Kevt'her Hoxha[1] · Sneha Narasimhan[1] · Lakshmi Changolkar[1] · Alyssa Rosenbloom[5] · Virginia M.-Y. Lee[1] · John Q. Trojanowski[1]

Received: 24 May 2019 / Revised: 9 July 2019 / Accepted: 18 July 2019 / Published online: 26 July 2019

Abstract

Identification of multiple immune-related genetic risk factors for sporadic AD (sAD) have put the immune system center stage in mechanisms underlying this disorder. Comprehensive analysis of microglia in different stages of AD in human brains revealed microglia activation to follow the progression of AD neuropathological changes and requiring the co-occurrence of beta-Amyloid (Aβ) and tau pathology. Carriers of AD-associated risk variants in TREM2 (Triggering receptor expressed on myeloid cells 2) showed a reduction of plaque-associated microglia and a substantial increase in dystrophic neurites and overall pathological tau compared with age and disease stage matched AD patients without TREM2 risk variants. These findings were substantiated by digital spatial profiling of the plaque microenvironment and targeted gene expression profiling on the NanoString nCounter system, which revealed striking brain region dependent differences in immune response patterns within individual cases. The demonstration of profound brain region and risk-variant specific differences in immune activation in human AD brains impacts the applicability of immune-therapeutic approaches for sAD and related neurodegenerative diseases.

Keywords Microglia · Alzheimer's disease · Neuropathology · TREM2

Introduction

Alzheimer's disease (AD) is the most common form of dementia that currently affects more than 30 million people worldwide [1]. Neuronal loss, extracellular deposition of beta-Amyloid (Aβ) and intracellular aggregation of tau protein are the characteristic neuropathological lesions in AD [2]. The accumulation of these neuropathological changes are accompanied by an activation of the brain's innate immune system, with microglia as the main cellular component [3]. Studies in animal models have contributed to expand our knowledge into how these cells are involved in disease pathogenesis and progression, but the complexity of the human disease condition, with multiple pathologies occurring at the same time [4], the long disease duration and evidence of significant differences in immune cell function and aging in humans when compared to animal models [5, 6] has hampered efforts to translate successful interventional paradigms to the human disease situation. The importance of immune cells in AD and related dementias (RD) has been underscored by the recent identification of several novel

Stefan Prokop and Kelly R. Miller contributed equally.

Electronic supplementary material The online version of this article (https://doi.org/10.1007/s00401-019-02048-2) contains supplementary material, which is available to authorized users.

✉ Stefan Prokop
sprokop@ufl.edu

✉ John Q. Trojanowski
trojanow@upenn.edu

1 Department of Pathology and Laboratory Medicine, AD Center Core (ADCC), Center for Neurodegenerative Disease Research, University of Pennsylvania (PENN) School of Medicine, Philadelphia, PA 19104, USA

2 Present Address: Department of Pathology, University of Florida, Gainesville, FL 32610, USA

3 Present Address: Center for Translational Research in Neurodegenerative Disease, University of Florida, Gainesville, FL 32610, USA

4 Present Address: Fixel Institute for Neurological Diseases, University of Florida, Gainesville, FL, USA

5 NanoString Technologies, Seattle, WA 98109, USA

genetic risk variants for sporadic AD (sAD) [7–9], Parkinson's disease (PD) [10], Frontotemporal dementia (FTD) [11] and disease causing mutations in rare familial forms of FTD [12]. The TREM2 receptor, one of the genetic variants associated with sAD has garnered particular interest due to the high increase in risk for sAD, despite its relatively low allele frequency [12]. Signaling through TREM2 is well known for modulating the activation of macrophages by promoting phagocytosis, reducing pro-inflammatory cytokine signaling and promoting cell survival [12, 13]. Similar functions seem to apply in microglia.

Studies in TREM2 knockout mice crossed to various mouse models exhibiting AD-like pathology have generated seemingly conflicting data [14–16]. It is now well accepted that TREM2 deficiency in animal models attenuates the immune response towards Aβ, which leads to structural changes in Aβ deposits, rendering them more toxic for the microenvironment and inducing neuritic tau pathology [17, 16]. Some of these findings have been correlated with analyses of patient derived brain specimens [18–16]; however, a comprehensive analysis of microglia in various brain regions and in patients carrying genetic risk variants in TREM2 has not been performed. Several factors hamper the translation of groundbreaking studies in mouse models to the human disease condition. First, most animal studies are performed in mice deficient in human TREM2 variants, while the AD-associated TREM2 variants are point mutations increasing AD risk in a heterozygous fashion [7, 8]. It is still not finally resolved if these risk variants are loss of function or toxic gain of function variants [19–22]. Second, most animal models only display one protein pathology, either Aβ or tau pathology, while the human disease condition is characterized by the co-occurrence of aggregates of both of these proteins [2]. Furthermore, due to prominent aging related differences between human and murine microglia [5, 6], the difference in disease duration between animal models and human subjects becomes a major factor impacting immune response patterns.

To overcome these drawbacks, we set out to perform a comprehensive analysis of microglia in AD in a disease stage, brain region and genetic risk-variant-specific manner. We combined conventional histological analysis with biochemical studies and multiplexed in situ protein analysis and gene expression profiling to provide a comprehensive analysis of the immune response patterns in human AD brains.

Materials and methods

Patient samples

Autopsy cases were selected from the Center of Neurodegenerative Disease Research (CNDR) at the University of Pennsylvania. The protocols for brain harvesting, selection of areas to obtain tissue blocks and staining and diagnostic procedures followed have been previously reported in detail [4, 23, 24].

Immunohistochemistry

For microglia profiling, 40 µm-thick sections were deparaffinized in descending order in xylene (2 × 10 min), 100% ethanol (10 min), 95% ethanol (10 min), 80% ethanol (10 min), 70% ethanol (10 min) and subsequently equilibrated to TBS (pH 7.6). All subsequent steps were performed on free-floating sections. Following treatment with methanol/H_2O_2 for 30 min and three washes in TBS (3 × 5 min), sections were incubated in blocking buffer (TBS with 2% FBS) for 30 min. Incubation with primary antibodies diluted in blocking buffer was performed over night at 4 °C. Following 5 washes with TBS, sections were incubated with biotinylated secondary antibody diluted in blocking buffer for 1–2 h at room temperature (RT). Following five washes with TBS sections were incubated with ABC reagent from Vecta 'Elite'kit solution for 30 min at RT. After five additional washes with TBS sections were developed with DAB according to manufacturer's instructions (Vector Laboratories 'DAB Substrate Kit for Peroxidase') between 1 and 10 min. After developing, sections were mounted on glass coverslips, counterstained with Hematoxylin for 30–60 s, dehydrated in ascending alcohol concentrations, and coverslipped with 24 × 50 coverslips using cytoseal mounting medium.

Staining of slide-mounted 5 µm-thick sections was performed as previously described [25].

Microglia analysis

Digital images of 40 µm-thick sections at 20 × magnification were obtained using a Lamina (Perkin Elmer, Waltham, MA) slide scanning system. Four representative images of respective anatomic regions were taken using Halo digital image software v1.90 (Indica Labs; Albuquerque, NM) and all microglia in the generated images were scored as homeostatic, activated, or dystrophic using ImageJ software. Percent of homeostatic, activated, and dystrophic microglia were recorded per region. Microglia numbers were counted in the respective regions using the manual counter module of the Halo software and the total number of microglia was calculated per mm^2.

Analysis of Aβ and tau burden and CD68 area covered

Anatomic regions of scanned slides stained for NAB228, PHF1, and CD68 were annotated using the Halo digital image software v1.90 (Indica Labs; Albuquerque, NM).

Only cortical areas were used for analysis. Area covered by DAB-positive staining was determined with the Halo software using the classifier module.

Quantification of neuritic plaques

Neuritic plaques were counted on PHF1 stained slides using the manual counting module of the Halo software in the same regions annotated for NAB228 and PHF1 area covered analysis and graphed in relation to the surface area of the counted region.

Biochemical analyses

Neuropathological hallmarks of AD in frozen frontal cortex human brain tissue samples from high AD and TREM2 patients were confirmed on a small portion of the frozen tissue sample, which was fixed and processed in formalin. The use of postmortem brain tissues for research was approved by the University of Pennsylvania's Institutional Review Board with informed consent from patients or their families. Extraction of PHF from 6 to 14 g of frontal cortical gray matter was performed following previously published protocols [25].

RNA isolation and analysis

Frozen tissue

RNA from frozen tissue specimens was isolated using the Trizol system according to manufacturer's protocols. Isolated RNA was purified using the Quiagen RNA easy kit according to manufacturer's instructions. RNA concentration was determined using Nanodrop and RNA quality was determined using the Bioanalyzer system with RNA pico chips according to manufacturer's instructions.

FFPE tissue

For RNA isolation from FFPE tissue, two 40 um-thick sections per region were deparaffinized by incubation in Xylene ($2 \times 10'$), 100% EtOH (10′), 95% EtOH (10′), 80% EtOH (10′), and 75% EtOH (10′) followed by a rinse in demineralized water. RNA from deparaffinized FFPE-tissue sections was extracted using the High Pure FFPET RNA Isolation Kit (Roche) according to manufacturer's protocols. RNA concentration was determined using the Nanodrop system and RNA quality was assessed with the Bioanalyzer system using RNA pico chips and the DV200 analysis module according to manufacturer's specifications.

Gene expression analysis

Gene expression analysis was performed using NanoString's human neuropathology and neuroinflammation gene expression panels (NanoString Technologies). RNA isolated from FFPE and fresh-frozen material was used for analysis. 100 ng of RNA from fresh-frozen material and 100 ng equivalent (adjusted for percent of fragmentation) served as input into the assay. Gene expression analysis was performed on the nCounter system (NanoString Technologies) according to manufacturer's instructions and analyzed using nSolver analysis software (NanoString Technologies) and built in statistical analyses.

NanoString digital spatial profiling

Formalin fixed paraffin embedded-tissue slides were deparaffinized as described above and incubated with a cocktail containing ~ 40 antibodies coupled with unique photocleavable oligonucleotide tags as well as four fluorescent markers. Amyloid beta plaques, microglia, and astrocytes were identified visually by fluorescently labeled antibodies against pan Amyloid Beta, HLA-DR, and GFAP, respectively (Novus). Nuclei were identified by staining with the nucleic acid-binding fluorescent dye, Syto13 (Thermo). Amyloid beta plaques for high-resolution multiplex profiling were selected by visual inspection. Using an early version of NanoString's GeoMx™ Digital Spatial Profiler system [26], for each plaque profiled, a single 100 µm circle was placed around the plaque core and two concentric donut-shaped rings were placed around the inner circle with 100/200 µm and 200/300 µm inner/outer diameters, respectively, highlighting the immediate plaque microenvironment. These selected areas were illuminated individually via UV light on GeoMx DSP, photocleaving the oligonucleotides present within each Region of Interest (ROI). The oligonucleotides were collected on GeoMx DSP in a 96-well microwell plate. Individual microwells containing the collected photocleaved oligonucleotides from each spatially resolved ROI were then hybridized to four-color, six-spot optical barcodes and analyzed on the nCounter® platform, resulting in distinct spatially mapped counts that correspond to the antibodies from which the tags were cleaved. Digital counts were first normalized with internal controls for system variation and then normalized to housekeeper protein counts and the specific ROI area.

Quantitative PCR (qPCR) analysis

Reverse transcription was performed using the Quantitect RT PCR kit (Qiagen) with 1 µg of total RNA as starting material according to manufacturer's instructions. cDNA was diluted 1:100 in RNAse free water and qPCR was performed on the

Qiagen system using the Fast master mix and the following Taqman (Thermo Fisher Scientific) detection probes: KCNJ 10 (Hs01922935_s1), TGFb1 (Hs00998133_m1), P2RX7 (Hs00175721_m1) and the housekeepers beta-Actin (Hs01060665_g1), UBC (Hs05002522_g1), and RPL13 (Hs00744303_s1). Raw gene expression data were normalized to the average of all three housekeepers using the ddCt method.

Graphpad prism7 was used for graphing of data and for statistical analysis.

Results

Microglial activation follows the progression of AD neuropathological changes

Evaluation of the effects of microglia-associated genetic risk variants in TREM2 in microglia activation across different stages of AD was accomplished through analysis of microglia morphology in a defined cohort of AD patient samples (Supplemental Table 1). To limit the number of variables in our analysis, we chose patients with only AD neuropathological changes and no concomitant or comorbid neuropathologies, including alpha-Synuclein, TDP-43 deposits, and hippocampal sclerosis, from our Center's Integrated Neurodegenerative Disease Database (INDD) [24, 27]. Hallmark pathological changes were confirmed by neuropathological assessment prior to inclusion into the study. Stages of AD pathology were defined according to the current diagnostic criteria for AD neuropathological changes [2] as no AD (12 cases), low AD (14 cases), intermediate AD (6 cases) and high AD (17 cases) pathology. In addition to these groups, we included a cohort of 17 patients carrying the AD-associated risk variants TREM2 p.R47H (15 cases) and TREM2 p.R62H (2 cases). All TREM2 cases exhibited high AD neuropathological changes, referred to as "high AD (TREM2)" or "TREM2" for the remainder of the manuscript. TREM2 cases were similar in average age and distribution of ApoE genotypes (Supplemental Table 1) to the cohort of patients with high AD neuropathological changes which did not carry the risk variants in the TREM2 locus, referred to as "high AD" for the remainder of the manuscript. To reflect the progression of AD neuropathological changes within an individual brain, we analyzed multiple brain regions for each patient. The section of the hippocampus sampled at the level of the lateral geniculated body, as well as subregions of the hippocampal formation, were chosen as a region affected in early stages of AD. The frontal cortex was included to reflect intermediate stage changes and the visual cortex, including striate and peristriate cortex, was included to analyze a brain region affected in late stages of AD neuropathology [23]. For the morphological analysis of microglia, we stained 40 µm-thick paraffin sections with the pan-microglia marker Iba1 [28], and scored the presence of three defined morphological stages of microglia [3]. Homeostatic microglia (Fig. 1a) are defined by modest cytoplasm and a complex and finely branched tree of thin processes. Activated microglia (Fig. 1b) show abundant cytoplasm with shortened, less branched and thicker processes and dystrophic/senescent microglia (Fig. 1c) are defined by fragmented and/or beaded processes, shrunken cytoplasm, and small irregular shaped nuclei with condensed chromatin [29, 30]. AD neuropathological changes, defined by Aβ deposits [31] and tau pathology [32, 33] increased across stages according to the staging scheme used for cohort definition [2]. Of note, we did not observe major differences in Aβ and tau pathology scores between high AD and TREM2 cases in the regions analyzed (Fig. 1g, k, o). Applying the microglia scoring scheme to our study cohort, we noted an increase in activated microglia (Fig. 1e) with progression of AD neuropathological changes in the hippocampus (Fig. 1g). This increase in activated microglia was mainly at the expense of homeostatic microglia (Fig. 1d) and a late stage increase in dystrophic microglia (Fig. 1f). Interestingly, we detected no differences in microglia morphologic states between high AD and TREM2 cases in the hippocampus. Detailed data for anatomical subregions of the hippocampal formation are available in Supplementary Fig. 1. We observed a similar progression of microglia activation in the frontal (Fig. 1h–j) and visual cortex (Fig. 1l–n). While there was again no difference between high AD and TREM2 cases in the frontal cortex, we observed a trend towards slightly lower microglia activation in the TREM2 cases when compared to high AD cases in the visual cortex (Fig. 1m). Dystrophic microglia were only observed in appreciable numbers in late stages of disease with abundant AD pathology in frontal cortex and visual cortex samples (Fig. 1j, n), but to a much lesser extent than in the hippocampal formation (Fig. 1f). The data obtained by morphological scoring of activated microglia were validated by analysis of CD68 stained tissue sections highlighting phagocytic microglia (Supplementary Fig. 2).

Microglia dystrophy/senescence shows regional variation and is enhanced in late stages of AD and by the presence of TREM2 risk variants

Analyzing the regional distribution of dystrophic microglia more closely, we noticed that this microglia phenotype was most abundant in the subiculum region of the hippocampal formation across all disease stages and overall more abundant in the hippocampal formation compared to the frontal and visual cortex (Fig. 2a). Furthermore, plotting the overall percentage of dystrophic microglia within each case across all regions demonstrated that dystrophic microglia increase with increasing stage of disease (Fig. 2b), in line with the

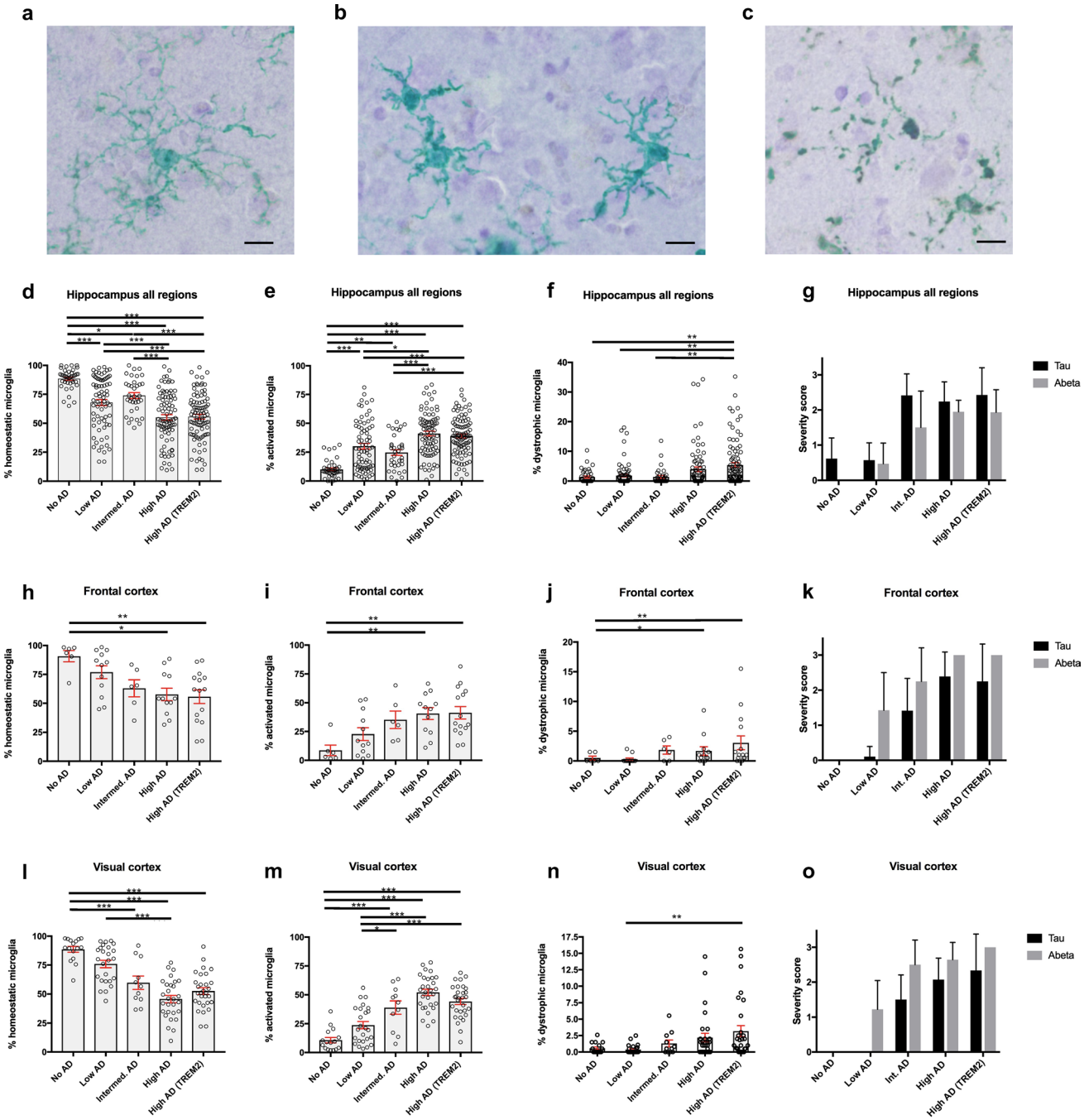

Fig. 1 Microglia activation follows the progression of AD neuropathological changes. Microglia morphology was scored in 40 µm-thick sections stained with Iba1 in the indicated anatomical regions as homeostatic (**a**), activated (**b**), and dystrophic (**c**). Percent of homeostatic, activated, and dystrophic microglia in the hippocampus (**d**–**f**), frontal cortex (**h**–**j**), and visual cortex (**l**–**n**), with each open circle representing the average score for the frontal cortex (No AD $n=6$, Low AD $n=12$, Int. AD $n=6$, High AD $n=12$, Trem 2 $n=15$ data points), representing the average score for striate and peristriate subregions per case for the visual cortex (No AD $n=16$, Low AD $n=25$, Int. AD $n=11$, High AD $n=29$, Trem 2 $n=30$ data points), and for the hippocampus, each open circle represents the average score in six individual anatomical subregions of the hippocampus per case (No AD $n=41$, Low AD $n=73$, Int. AD $n=35$, High AD $n=83$, Trem2 $n=94$ data points). Light gray bars represent the mean and red error bars depict ± standard error of mean. Scoring of AD pathology in three tier scoring system (mild = 1, moderate = 2, severe = 3, see also Supplemental Fig. 2) in the hippocampus (**g**), frontal cortex (**k**), and visual cortex (**o**) with solid black bars representing tau pathology and gray bars representing Aβ pathology (No AD $n=13$, Low AD $n=14$, Int. AD $n=6$, High AD $n=18$, Trem2 $n=16$). One-way ANOVA with Bonferroni posttest was used for statistical analysis. $*p<0.05$, $**p<0.01$, $***p<0.001$. Scale bar = 10 µm

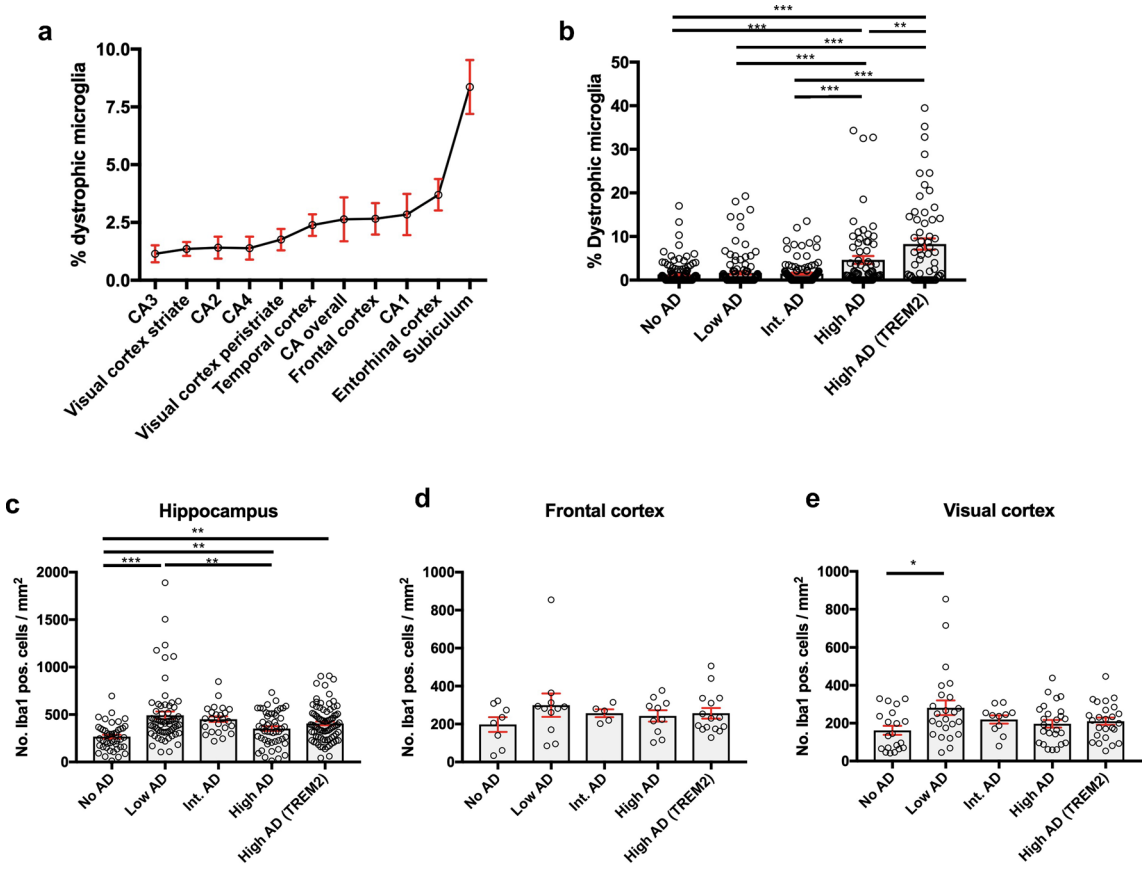

Fig. 2 Microglia dystrophy appears in late disease stages and microglia numbers vary throughout anatomical regions and disease stages. **a** Average percentage of dystrophic microglia per anatomical region combined for all disease stages (frontal cortex $n=57$, visual cortex striate $n=60$, visual cortex peristriate $n=63$, temporal cortex $n=54$, entorhinal cortex $n=52$, subiculum $n=54$, CA overall $n=55$, CA1 $n=53$, CA2 $n=51$, CA3 $n=51$, CA4 $n=53$ and cerebellum $n=58$). **b** Average percentage of dystrophic microglia per disease stage, combined for all anatomical regions per case (No AD $n=139$, Low AD $n=130$, Int. AD $n=120$, High AD $n=69$ and Trem2 $n=59$). Microglia numbers (per mm^2) in the hippocampus (**c**), frontal cortex (**d**), and visual cortex (**e**). Each open circle represents microglia numbers for one case for the frontal cortex (No AD $n=8$, Low AD $n=11$, Int. AD $n=5$, High AD $n=10$ and Trem2 $n=15$), for the hippocampus each circle represents microglia numbers per subregion (No AD $n=45$, Low AD $n=65$, Int. AD $n=24$, High AD $n=51$ and Trem2 $n=83$ data points) and for the visual cortex each circle represents microglia numbers per subregion (No AD $n=20$, Low AD $n=24$, Int. AD $n=11$, High AD $n=26$ and Trem2 $n=25$ data points). Light gray bars represent the mean and red error bars depict ± standard error of mean. One-way ANOVA with Bonferroni posttest was used for statistical analysis. $*p<0.05$, $**p<0.01$, $***p<0.001$

notion that this microglia phenotype is induced by long standing, chronic activation due to accumulating AD pathology [29], which is prevalent in late disease stages and in the hippocampal formation. Interestingly, however, dystrophic microglia were significantly more abundant in TREM2 cases (Fig. 2b), compared to high AD cases, indicating that this genetic risk variant alters the functional state of microglia, in particular with respect to long-term chronic activation.

Microglia numbers are regionally different, increase in early stages of disease and decline in late stages

Besides the different morphological stages of microglia, we also analyzed microglia numbers in our study cohort. In line with the previous publications [34], microglia numbers differed across the anatomical regions we analyzed (Fig. 2c–e) with higher microglia numbers in the hippocampus compared to frontal and visual cortex. We observed an increase in microglia numbers in early stages of disease in all the regions analyzed (Fig. 2c–e), reflecting increasing activation and proliferation of these cells in response to ensuing AD pathology. However, the upward trend in microglia numbers subsided in intermediate disease stages and led to reduced microglia numbers in high AD cases, which was previously reported and assumed to be due to toxicity of soluble tau species on microglia [29]. This decrease in microglia numbers was not apparent in TREM2 cases, again supporting the notion of altered microglia activation status in the TREM2 risk-variant

carriers which ties in with the presence of more dystrophic microglia in TREM2 cases (Fig. 2b).

Microglia activation requires the co-occurrence of Aβ- and tau pathology

To dissect a potential differential impact of Aβ- and tau pathology on microglia activation, we analyzed additional cohorts of patients with only select pathological protein deposits (Supplementary Table 1). We first analyzed the impact of AD-associated tau pathology on microglia activation in hippocampal samples from patients with the pathological diagnosis of primary age-related tauopathy (PART [35], four cases), exhibiting high levels of AD-associated tau pathology confined largely to temporal lobe without significant Aβ pathology. Since we did not observe differences in the morphologies of activated microglia between high AD and TREM2 cases, we combined these two disease groups as "high AD" for the purpose of this analysis. As expected, PART cases show high levels of tau pathology in the form of neurofibrillary tangles and neuropil threads with no concurrent Aβ pathology, and high AD cases are characterized by the co-occurrence of high levels of Aβ- and tau pathology (Fig. 3b). While high AD cases showed a substantial increase in activated microglia when compared to controls, we did not observe a notable increase in microglia activation in PART cases (Fig. 3a), indicating that tau pathology alone, in the absence of co-occurrent Aβ-pathology is not sufficient to induce substantial microglia activation. Analysis of dystrophic microglia in this cohort revealed similar results, with no increase in microglia dystrophy in PART cases compared to controls (data not shown). To analyze microglia activation in the presence of only Aβ-deposits, we analyzed frontal cortex samples of patients with high Aβ plaque burden, but no to minimal tau pathology, referred to as "pathological aging" cases [36] (12 cases), and we compared those samples to our high AD and control groups (Fig. 3d). Similar to the situation with only tau pathology in the hippocampus of PART patients, we observed no major increase in microglia activation over controls in pathological aging patients, while high AD patients showed a substantial increase in microglia activation (Fig. 3d). Of note, both the PART cohort and the pathological aging cohort had a significantly higher average age than the control group, demonstrating that the

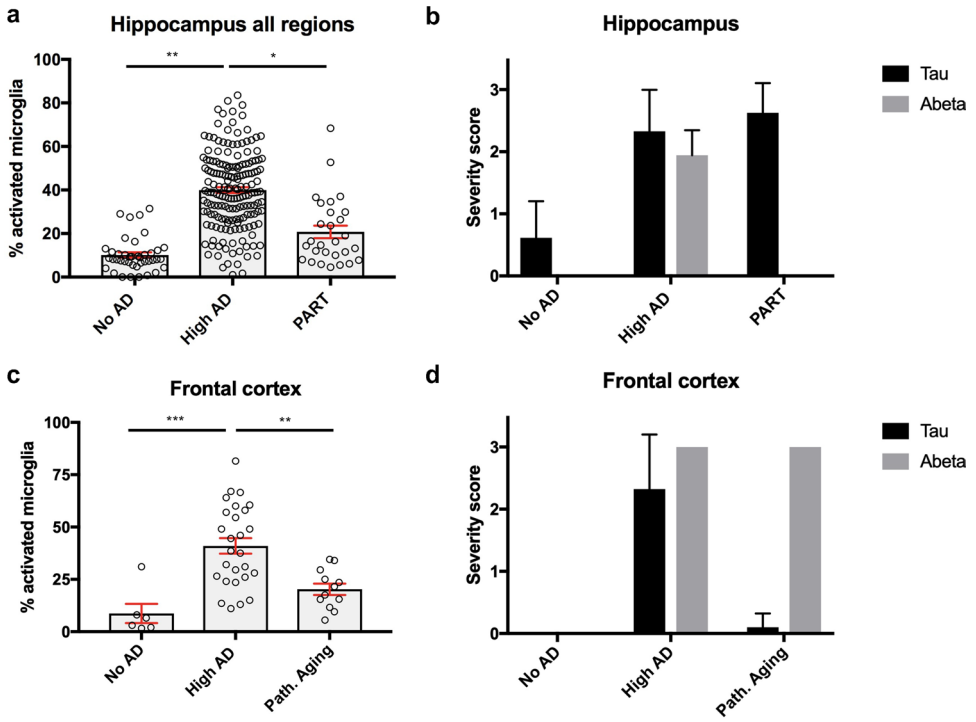

Fig. 3 Microglia activation depends on the co-occurrence of Aβ and Tau pathology. Percent activated microglia for the hippocampus (**a**) and frontal cortex (**c**). Each open circle represents the average percent of activated microglia for the anatomical region (frontal cortex) or across all subregions (hippocampus). "High AD" combines the scores for high AD cases and Trem2 cases. Hippocampus (No AD $n=41$, High AD $n=177$ and PART $n=28$ data points) and Frontal cortex (No AD $n=6$, High AD $n=27$ and Pathological aging $n=12$). Light gray bars represent the mean and red error bars depict ± standard error of mean. **b**, **d** Aβ-pathology (gray bars) and tau pathology (black bars) for experimental groups and anatomical region (hippocampus: No AD $n=13$, high AD $n=34$, PART $n=4$; frontal cortex: No AD $n=13$, high AD $n=34$ and path. aging $n=12$). One-way ANOVA with Bonferroni posttest was used for statistical analysis. $*p<0.05$, $**p<0.01$, $***p<0.001$

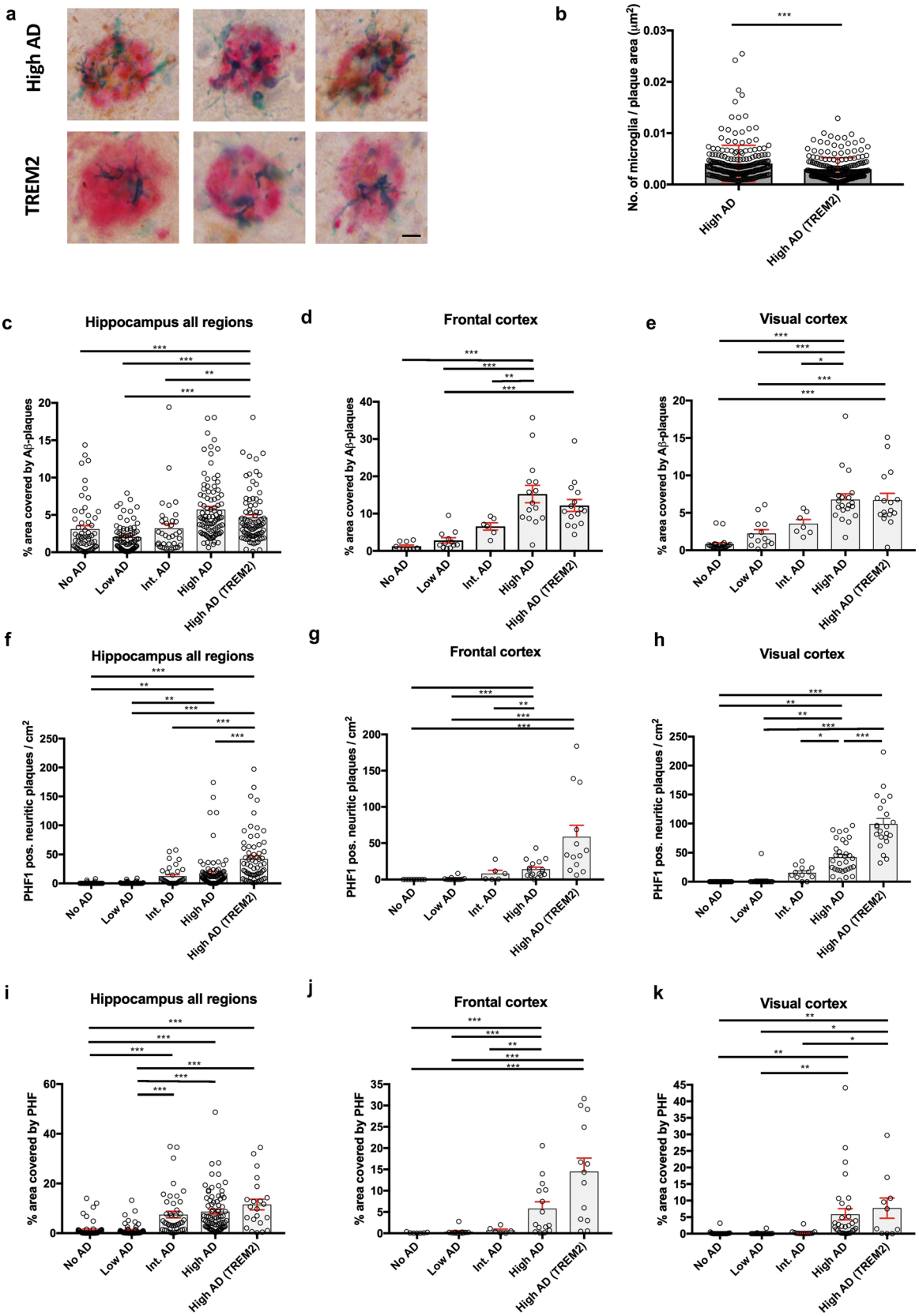
a
High AD
TREM2
b
No. of microglia / plaque area (µm²)
High AD
High AD (TREM2)
c
Hippocampus all regions
% area covered by Aβ-plaques
d
Frontal cortex
% area covered by Aβ-plaques
e
Visual cortex
% area covered by Aβ-plaques
f
Hippocampus all regions
PHF1 pos. neuritic plaques / cm²
g
Frontal cortex
PHF1 pos. neuritic plaques / cm²
h
Visual cortex
PHF1 pos. neuritic plaques / cm²
i
Hippocampus all regions
% area covered by PHF
j
Frontal cortex
% area covered by PHF
k
Visual cortex
% area covered by PHF
No AD
Low AD
Int. AD
High AD
High AD (TREM2)

◂**Fig. 4** Reduction in plaque-associated microglia, increased neuritic plaques and increased overall tau pathology in TREM2 variant carriers. **a** Representative photomicrographs of plaque-associated microglia (Aβ, red, Nab228 stain; microglia, green, Iba1 stain). Upper row high AD cases, lower row TREM2 cases. Scale bar = 10 µm. **b** Quantification of number of microglia per plaque area (µm^2). Each symbol represents number of microglia for one plaque. ***$p > 0.001$, Mann-Whitney test. **c**–**e** Percent covered by Aβ plaques (Nab228 stain) for all anatomical subregions of the hippocampus (**c**), frontal cortex (**d**), and all subregions of the visual cortex (**e**). Each circle represents average percentage of Aβ covered areas per anatomical region per case, including anatomical subregions for hippocampus and visual cortex. **f**–**h** Number of neuritic plaques per cm^2 (PHF1 stain) for all anatomical subregions of the hippocampus (**f**), frontal cortex (**g**), and all subregions of the visual cortex (**h**). Each circle represents average number of neuritic plaques per anatomical region per case, including anatomical subregions for hippocampus and visual cortex. **i**–**k** Percent area covered by pathological tau (PHF1 stain) for all anatomical subregions of the hippocampus (**f**), frontal cortex (**g**), and all subregions of the visual cortex (**h**). Each circle represents average percent area covered by PHF1 stain per anatomical region per case, including anatomical subregions for hippocampus and visual cortex. One-way ANOVA with Bonferroni posttest was used for statistical analysis. *$p < 0.05$, **$p < 0.01$, ***$p < 0.001$

observed increases in microglia activation in high AD cases are mainly due to the presence of co-occurrent Aβ- and tau pathology and not merely an effect of advanced age.

TREM2 variants reduce microglial accumulation around plaques and are associated with higher pathological tau burden

Since we did not observe major differences in the percentage of activated microglia in TREM2 and high AD cases (Fig. 1), but saw profound changes in the amount of dystrophic microglia and microglia numbers between these two experimental groups, we undertook a more detailed analysis of the spatial relationship of microglia and Aβ-plaques. In line with the previous reports in mouse models [15–17] and human specimens [16], we observed a reduction in plaque-associated microglia in TREM2 cases when compared to high AD cases in the frontal cortex (Fig. 4a, b). This limited burden of plaque-associated microglia has been proposed to reduce the microglia barrier function around Aβ deposits and enhance toxicity of plaques [17, 16]. Since the four-tier scoring system that is commonly used to quantitate pathology in neurodegenerative diseases (see Supplementary Fig. 3a) depicted in Figs. 1 and 3, did not reveal major differences between high AD and TREM2 cases, we performed a more detailed computer-assisted image analysis (Indica labs, Supplementary Fig. 3b, c). As expected, the analysis of the % area covered by Aβ deposits showed an increased accumulation of aggregated Aβ with progression of AD neuropathological stages in all the anatomical regions we analyzed (Fig. 4c–e), but did not reveal any differences in Aβ deposition between high AD and TREM2 cases. In fact, we observed a trend towards slightly less Aβ deposits in TREM2 compared to high AD cases. This changed dramatically when we looked at the number of neuritic plaques (Fig. 4f–h) and area covered by phosphorylated tau protein (Fig. 4i–k) that are effectively highlighted by PHF-1 immunohistochemical staining. Both parameters showed the expected increase with progression of disease stages, but here, we noted a significantly higher burden of neuritic plaques (Fig. 4f–h) and overall area covered by phosphorylated tau in TREM2 compared to high AD cases (Fig. 4i–k). These findings were most pronounced in the frontal cortex (Fig. 4d, g, j) but consistently observable in the other brain regions included in our study (Fig. 4c, e, f, h, I, k).

To better quantitate the differences between high AD and TREM2 cases with respect to pathological proteins, we isolated insoluble tau and Aβ from frozen frontal cortex samples of selected patients (see Supplementary Table 2) included in our histological analysis using established protocols [25, 36]. Prior to homogenization of the frozen tissue, a representative portion of the frozen tissue sample was dissected, fixed in formalin, embedded in paraffin, and neuropathological changes (Aβ- and tau pathology) were compared to the initial formalin fixed paraffin embedded (FFPE) tissue portion utilized for the histological analysis detailed above. Western blot analysis of total tau protein in the homogenate revealed no differences between high AD and TREM2 cases, but we observed a substantial increase in insoluble, phosphorylated tau in TREM2 compared to high AD cases (Fig. 5a–c). Quantitation of insoluble Aβ by ELISA also corroborated our histological analysis by revealing no major differences in Aβ burden between high AD and TREM2 cases (Fig. 5h, k, n). In line with the notion that the reduced microglia barrier function in TREM2 cases increases the propensity of Aβ to induce phosphorylated tau pathology, we observed a significant increase in the ratio of insoluble phosphorylated tau and insoluble Aβ in TREM2 compared to high AD cases (Fig. 5g–o).

Analysis of the plaque microenvironment using the Nanostring GeoMx platform reveals important differences between high AD and TREM2 cases

To further elucidate the differences between high AD and TREM2 cases with respect to plaque microenvironment, we took advantage of the NanoString GeoMx platform to get a detailed view of > 40 proteins simultaneously in the plaque microenvironment with digital quantitation and spatial resolution. We selected frontal cortex sections from six patients per experimental group and analyzed three concentric circles around 10–20 dense cored Aβ plaques per section (Fig. 6a, b), reflecting distinct portions of the plaque microenvironment. Radial heat maps of the protein changes highlight the profound differences in the plaque microenvironment

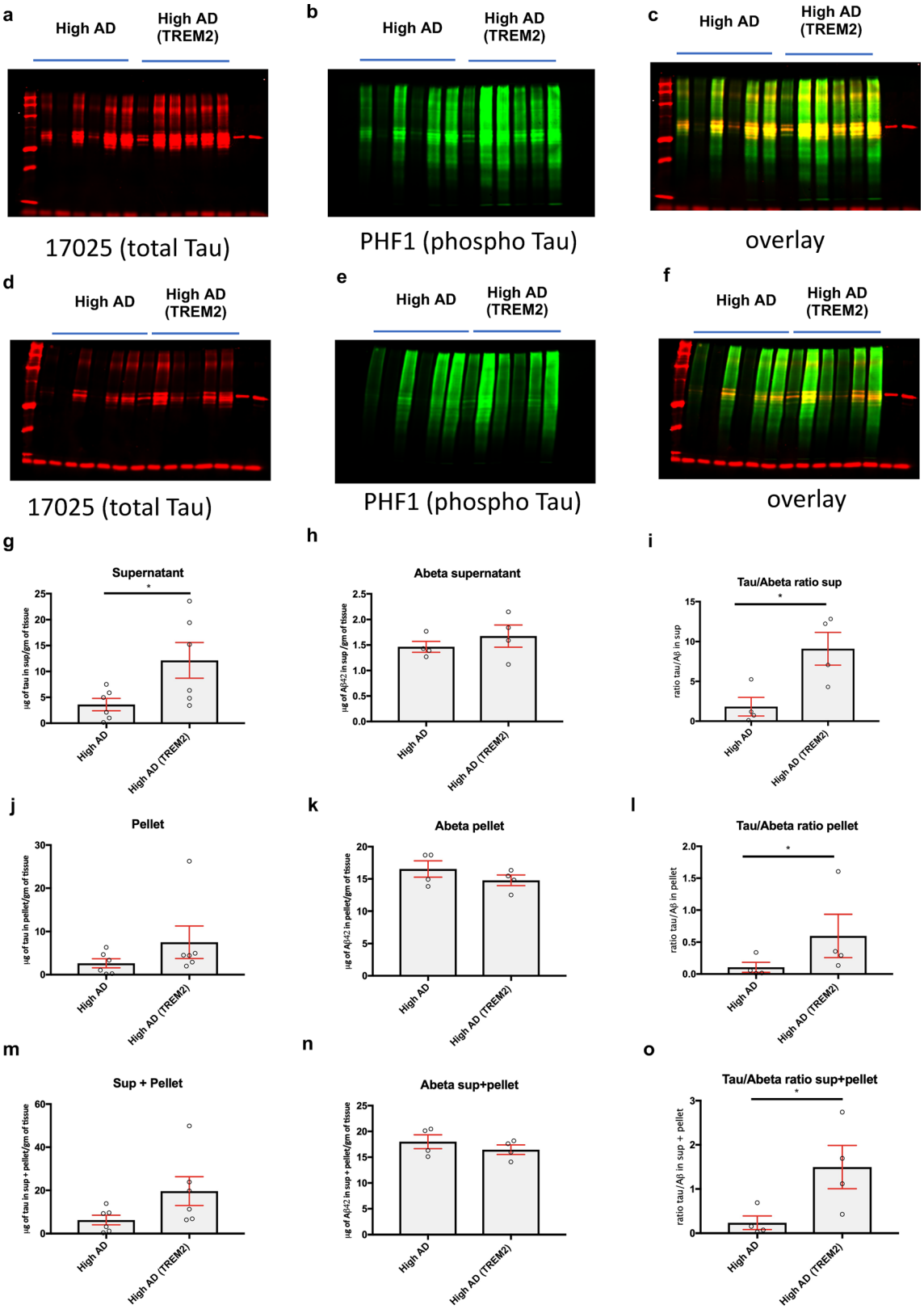

between high AD and TREM2 cases (Fig. 6a, b). This is further substantiated by unbiased clustering of the multiplexed protein data which reveals a greater similarity between the plaque centers (Mask 1) versus the more peripheral areas across both groups (Masks 2 and 3), while still exhibiting substantial differences in a multitude of proteins nearest

◂**Fig. 5** Increased ratio of insoluble Tau to Aβ in TREM2 cases. Western blot analysis of insoluble tau in the final supernatant (**a**–**c**) and pellet (**d**–**f**) of protein extraction. **a**, **d** Total tau (17,025, red), **b**, **e** phosphorylated tau (PHF1, green), and (**c**, **f**) overlay. Quantification of insoluble tau in final supernatant (**g**) and pellet (**j**) as well as total insoluble tau (supernatant + pellet, **m**). Insoluble Aβ42 quantified by ELISA in final supernatant (**h**), final pellet (**k**), and total (supernatant + pellet, **n**). Ratio of insoluble tau and insoluble Aβ42 in final supernatant (**i**), final pellet (**l**) and combined total (supernatant + pellet, **o**). *$p < 0.05$, unpaired Student's *t* test

to the plaque compared between the two groups (Fig. 6c). Indeed, the two areas more distant from the plaque center showed even more profound differences with TREM2 and high AD clustering separately and exhibiting multiple altered protein products (Fig. 6c).

Analyzing individual proteins in more detail, we confirmed an increase of tau protein and phosphorylated tau (pSer396/pSer404) epitope in all the regions around the plaque (Fig. 6d), in line with our conventional histological (Fig. 4g, j) and biochemical data (Fig. 5a–c). As expected, we observed no difference in Aβ40 and Aβ42 levels between the experimental groups (Fig. 6e), also in line with our conventional histological (Fig. 4d) and biochemical data (Fig. 5e). Analyzing the regional abundance of the proteins in more detail, we noted an expected higher abundance of Aβ40 and Aβ42 in the plaque center compared to the periphery (Supplementary Fig. 4b). In addition to Aβ40 and Aβ42, markers for microglia (CD68 and HLA-DR), as well as the proliferation marker Ki-67 were more abundant in the plaque center (Supplementary Fig. 4b), reflecting more pronounced microglia activation closer to the plaque center core. Further inspection also revealed higher levels of NMDAR and synaptophysin, as well as S100B in TREM2 cases compared to high AD cases (Supplementary Figs. 4a, 5a, c, d), while calbindin was significantly less abundant in the plaque microenvironment of TREM2 cases compared to high AD (Supplementary Figs. 4a, 5e).

Genetic screening of archival FFPE-tissue samples using NanoString nCounter platform

Given that we were able to define profound differences between TREM2 and high AD cases with respect to dystrophic neurites, overall tau burden, and the composition of the Aβ plaque microenvironment, despite the fact that our morphological analysis of microglia did not reveal major differences between these two groups, we sought to employ the NanoString nCounter platform to interrogate gene expression profiles in our cohorts. Given the typically poor quality of RNA from FFPE material, we first tested the robustness of the assay across a wide array of post mortem tissue samples. Raw data counts derived from the nCounter assay were comparable among a broad range of post mortem intervals (Supplementary Fig. 6a), indicating no major effect of post mortem interval (and RNA degradation) on gene expression data. Furthermore, we compared gene expression profiles derived from FFPE tissue with profiles generated from the corresponding frozen tissue specimens of the same case/brain region and noted an excellent correlation between gene expression profiles derived from frozen and FFPE tissue (Supplementary Fig. 6b). Turning our attention to changes in individual genes, we compared differential expression data obtained on the NanoString platform from FFPE tissue with gene expression profiles generated by conventional quantitative PCR (qPCR) performed on RNA isolated from frozen tissue specimens corresponding to the FFPE material used for the NanoString analysis. We observed similar changes in the subset of genes tested across the NanoString platform and qPCR (Supplementary Fig. 6c–f). Moreover, cell-type profiling with the NanoString nCounter platform correlated well with conventional analysis as shown for microglia activation (Supplementary Fig. 6g) and biochemical analysis of markers of neuronal integrity (Supplementary Fig. 6h) demonstrating that the NanoString nCounter platform provides robust and reliable data from post mortem FFPE brain tissues.

Gene expression profiling reveals distinct pathway and cell-type changes in TREM2 variant carriers

We compared expression of nearly 1540 genes across NanoString's Neuropathology and Neuroinflammation gene expression panels in matched hippocampal, frontal cortex, and visual cortex samples from high AD and TREM2 cases in relation to control specimens. Both high AD and TREM2 cases showed profound and significant changes in multiple genes when compared to controls (Supplementary Figs. 7, 8). We validated some of the significantly altered genes by qPCR analysis performed on RNA isolated from corresponding frozen tissue specimens also used for the biochemical analysis described above (Supplementary Figure 6c–e). While the direct comparison between high AD and TREM2 demonstrated changes in multiple genes, none of the individual genes reached statistical significance (Supplementary Tables and Supplementary Fig. 9). However, plotting pathway scores derived from the Neuropathology panel in high AD and TREM2 cases uncovered profound differences in multiple pathways across the brain regions we analyzed (Fig. 7a, b and Supplementary Tables 3–7). We observed higher immune activation scores and lower scores of pathways associated with synaptic function and neuronal density in the hippocampus, where neuropathological changes are present for the longest time [23], and therefore, the most profound effects on synaptic and neuronal integrity are expected. On the other hand, these pathway scores were generally much lower in the visual cortex, where

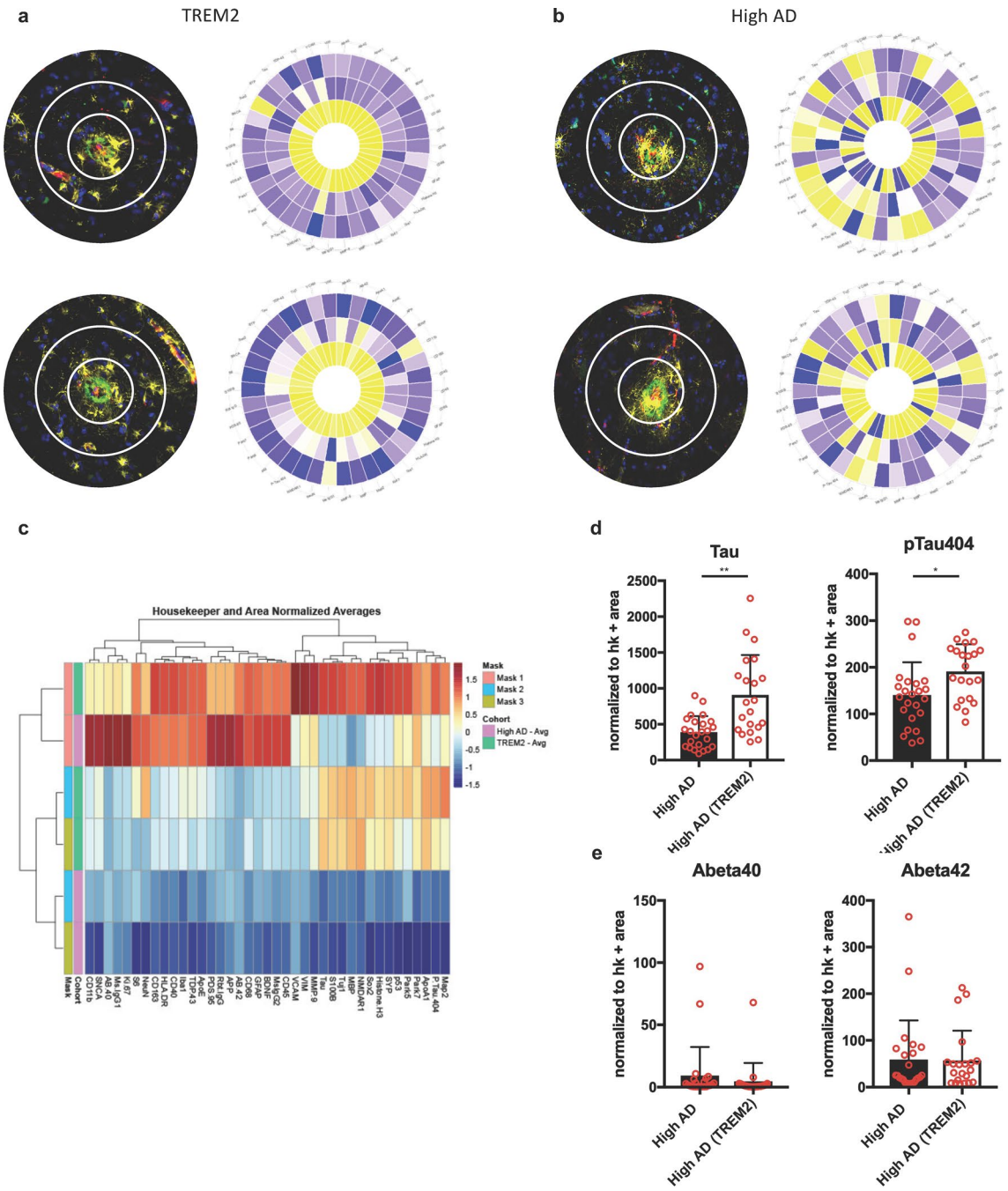

Fig. 6 Altered plaque microenvironment in TREM2 cases. Targeting images (**a**, **b**, left row) for multiplexed protein analysis (green = Aβ, yellow—Iba1, blue = nuclei) with three concentric circles around the plaque center. **a**, **b** Radial heatmaps of protein quantification within three regions around the plaque center for TREM2 (**a**, right row) and high AD (**b**, right row). **c** Heat map of unbiased clustering of multiplexed protein data for both experimental groups and concentric regions around plaque center. Color legend for relative protein expression and experimental group/zone. Mask1 refers to plaque center, Mask2 refers to middle ring and Mask3 refers to outer most ring for each plaque. **d** Graphical representation of protein data for phosphorylated tau (pSer396/pSer404) for high AD (black bars) and TREM2 (white bars) per concentric region around plaques. Red circles represent average protein data per case per region. Error bars represent standard error of mean. **e** Graphical representation of protein data for Aβ42 for high AD (black bars) and TREM2 (white bars) per concentric region around plaques. Red circles represent average protein data per case per region. Error bars represent standard error of the mean

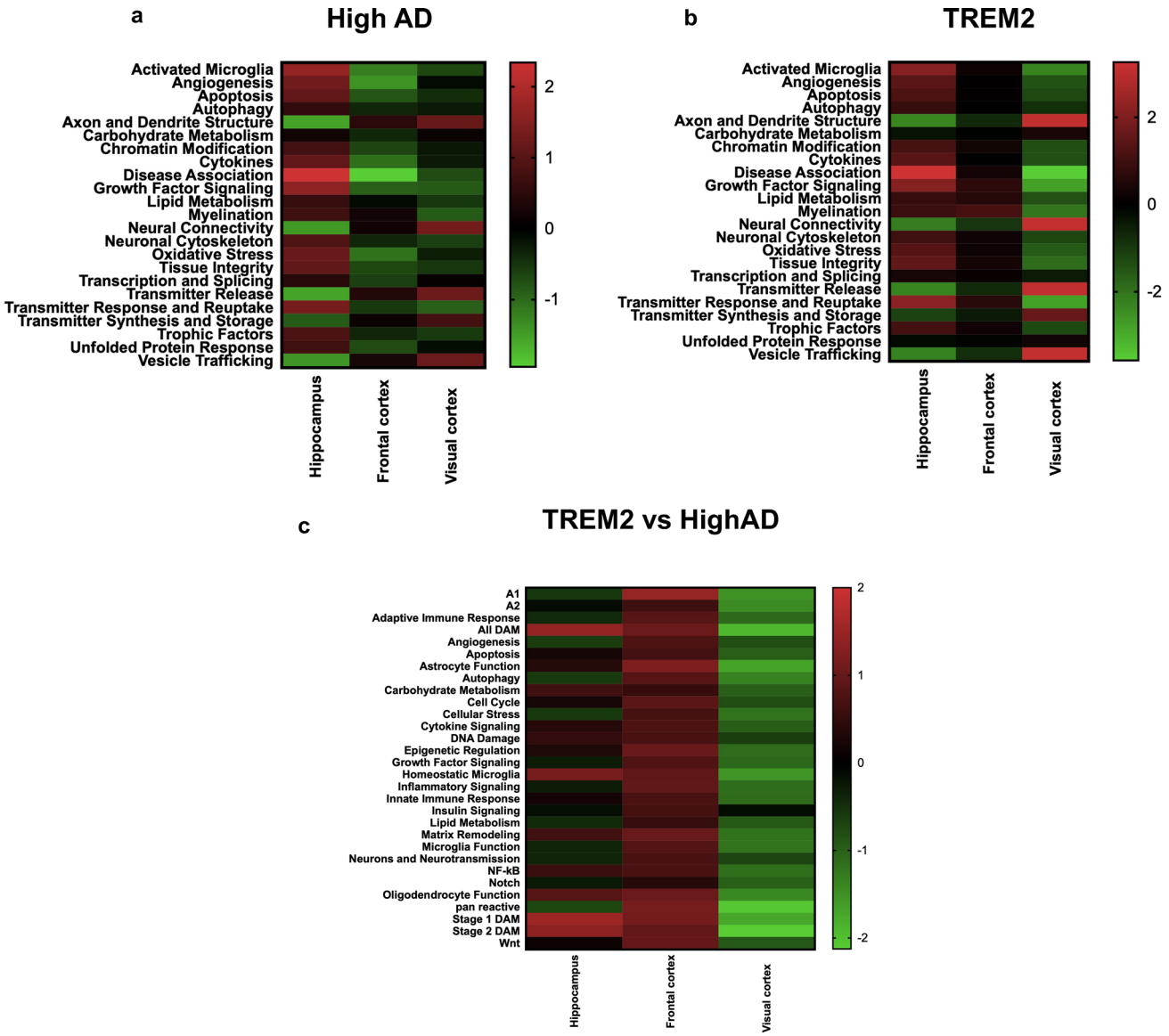

Fig. 7 Differences in gene expression patterns in different anatomical regions and TREM2 variant carriers. **a**, **b** Heatmap of average pathway scores derived from the nCounter Neuropathology panel for hippocampus, frontal cortex and visual cortex in high AD cases (**a**, $n=6$ per region) and TREM2 (**b**, $n=6$ per region). **c** Heatmap of weighted pathway scores (GSA analysis) derived from the nCounter Neuroinflammation panel in TREM2 cases over High AD cases for hippocampus, frontal cortex and visual cortex ($n=10$ per group for frontal cortex, $n=6$ per group for hippocampus and $n=4$ per group for visual cortex)

pathological changes are thought to be present for the shortest period of time. Although similar trends in pathway scores were noted between the different brain regions for high AD and TREM2, we also noted differences between the general patterns between these two experimental groups.

To further dissect these differences, we analyzed samples of hippocampus, frontal cortex, and visual cortex with the nCounter Neuroinflammation panel. We performed gene set analysis (GSA) of pathway scores for the comparison of high AD and TREM2 in each anatomical region (Fig. 7c) and found striking differences between high AD and TREM2 cases, which further showed opposing trends in different brain regions analyzed. Pathways associated with astrocytic activation ("pan reactive", "A1" and "A2" [37, 38]), and microglia activation ("all DAM", "stage1 DAM" and "stage2 DAM", [39]) were downregulated in the visual cortex of TREM2 compared to high AD cases (Fig. 7c, 8c), in line with the trend towards a lower percentage of activated microglia observed in the visual cortex in our histological analysis (Fig. 1m), despite comparable protein pathology (Fig. 1o). In contrast, TREM2 cases exhibited a more "pro-inflammatory" profile in the frontal cortex (Fig. 7c) with

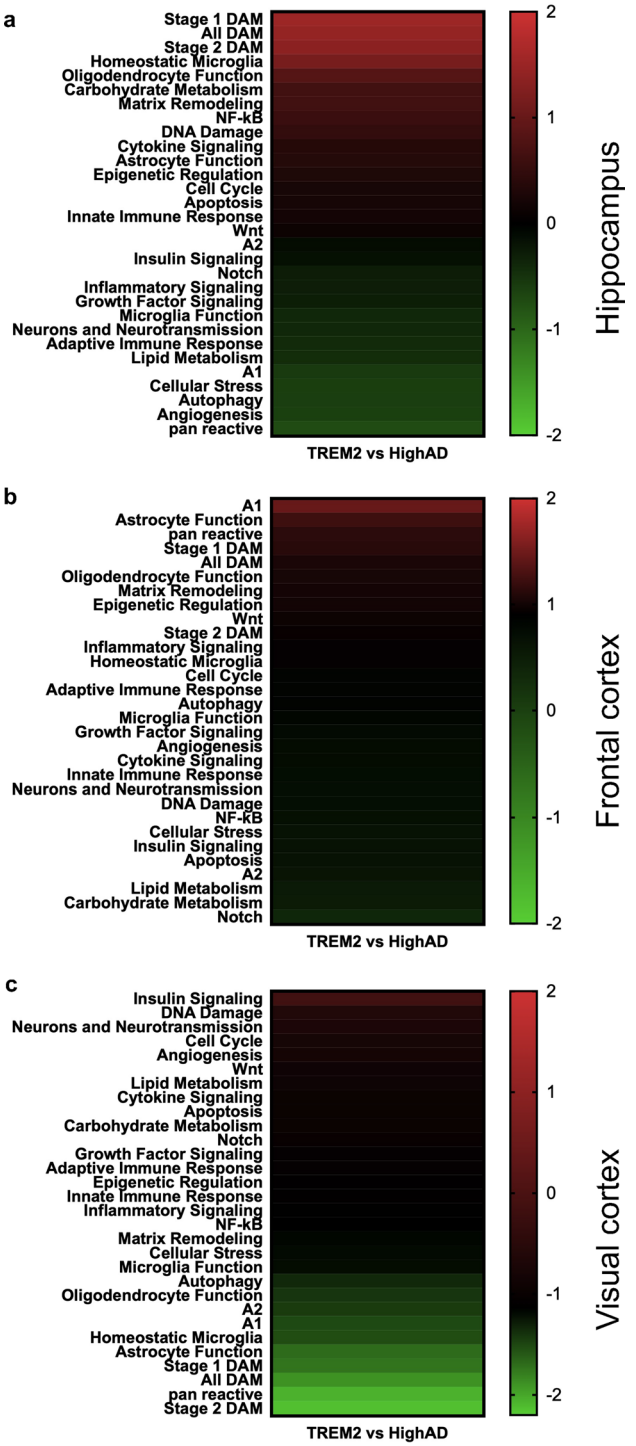

Fig. 8 Differences in immune response patterns between high AD and TREM2 cases depend on the anatomical brain region. **a**–**c** Heatmap of weighed average pathway scores derived from the nCounter Neuroinflammation panel for high AD and TREM2 cases in the hippocampus (**a**), frontal cortex (**b**) and visual cortex (**c**). Pathway scores are depicted in descending order of differential regulation in TREM2 cases over High AD cases

astrocyte ("pan reactive", "A1" and "astrocyte function") and microglia-associated pathways ("all DAM" and "stage1 DAM") being upregulated compared to high AD (Fig. 8b). In the hippocampus, the picture was less well-delineated with microglia-associated pathways being again upregulated in TREM2 cases ("all DAM", "stage1 DAM" and "stage2 DAM"), but astrocyte related scores ("pan reactive" and "A1") being lower than in high AD cases (Fig. 8a).

Discussion

In the present study, we undertook a detailed and multimodal analysis of immune activation in a cohort of sporadic AD patients at different disease stages including a cohort of patients carrying AD TREM2 genetic risk variants. In an initial morphological analysis, we observed an increase in activated microglia following the progression of AD neuropathological changes, namely, Aβ- and tau pathology, in all anatomical brain regions included in our study. Importantly, we did not observe substantial microglia activation in brain regions which were not yet affected by pathological protein aggregates, such as the frontal cortex in subjects with low AD neuropathological changes or the visual cortex of subjects with low and intermediate AD neuropathological changes. This argues against an initial precipitating role of immune activation in the cascade of AD-associated changes, but rather favors the concept that immune activation follows the protein pathology and potentially modulates it's extent and progression in later stages of disease [40], termed the "cellular phase" by some authors [41]. Interestingly, we did not observe significant microglia activation in cases with only AD-associated tau inclusions and no substantial Aβ deposits in the hippocampus (PART cases) or only Aβ deposits in the frontal cortex without substantial tau pathology (pathological aging cohort). In contrast, co-occurrence of Aβ- and tau pathology associated with microglia reactivity indicating that neuronal injury, most prominently dystrophic neurites, was strongly associated with an increase in microglia activation. These findings again support the notion, that—at least initially—the innate immune system responds to damage inflicted by pathological proteins and later acts to modulate the toxicity and progression of these aggregates. These data are also important with respect to studies analyzing the impact of purified Aβ and tau on microglia in culture, which most likely do not reflect a physiologically relevant phenomenon.

Microglia activation was associated with an increase in microglia numbers in early stages of AD, which is well in line with the known response pattern of microglia and observations in animal models [3]. However, in later disease stages, and most pronounced in the hippocampus of high AD patients, we observed a reduction in microglia numbers

compared to no AD controls. This phenomenon has been described in a previous study and was suggested to be due to toxicity of certain tau species on microglia [42]. Interestingly, TREM2 cases did not show the drop of microglia numbers we observed in high AD cases, despite increased pathological tau burden.

Microglia dystrophy, which is reflective of cellular senescence, has been described as a phenomenon observed upon chronic stimulation of microglia in conjunction with AD neuropathological changes, aging, and repeated injury or chronic stimulation [29]. We provide for the first time a systematic and quantitative assessment of microglia senescence across different brain regions and show the dependence of this on the progression of AD neuropathological changes. In line with the notion that microglia senescence occurs after repeated and long-term stimulation [29], an increase of dystrophic microglia was mainly seen in late disease stages and was most pronounced in the hippocampal formation, a region affected already in early stages of disease. While we appreciated the presence of senescent microglia as a constant finding, especially in higher disease stages, the overall percentage of dystrophic microglia was only in the low 10% range for most brain regions and exceeded 20% only in the subiculum. Interestingly, however, we noticed a significantly higher percentage of dystrophic microglia in TREM2 cases when compared to high AD cases. This phenomenon is likely due to differences in microglia metabolism and activation between high AD and TREM2 cases, as has been suggested by animal studies [13, 43–48]. This theory is further supported by the findings described above, with preserved microglia numbers in TREM2 cases in late disease stages. While this increase in dystrophic microglia may seem to reflect greater cellular stress in TREM2 risk carriers at first glance, another more plausible explanation which is more consistent with the data presented herein regarding microglia activation and inflammation in TREM2 carriers, wherein we showed that microglia are less activated in TREM2 variant cases and, therefore, become senescent at a later stage in the disease course. This suggests that microglia are present at higher numbers simply, because they have not yet died and been eliminated, as has presumably occurred in high AD cases, where microglia are more aggressively activated. Another possibility is that these cells may have entered a state of cellular senescence in which they are maintained in a dysfunctional state rather than undergoing cell death as appears to happen in high AD cases. The impact of senescent microglia in disease pathogenesis and progression remains unclear, but a recent study in a mouse model suggested that the removal of all senescent cells prevented progression of tau pathology [49], making this microglia phenotype a potential target for therapeutic intervention.

One constant finding across multiple studies of the effect of TREM2 deficiency on Aβ is a reduction in plaque-associated microglia, that appeared to associate with a reduced microglia barrier function and increase in dystrophic neurites [14, 16–18, 22, 50, 51]. We expand the finding of the previous studies focused on the frontal cortex [16] by demonstrating a reduction in plaque-associated microglia in frontal cortex and increased neuritic plaque burden in hippocampus, frontal cortex, and visual cortex of TREM2 cases compared to high AD cases. This increase in neuritic plaques in TREM2 cases was accompanied by an increase in overall area covered by phosphorylated tau and an increase of insoluble tau burden with similar levels of insoluble Aβ. These results tie in well with the above described findings in animal models and provide further evidence that AD-associated TREM2 variants increase the toxicity of Aβ deposits which leads to an increased burden of phosphorylated tau compared with AD cases without TREM2 variant and similar insoluble Aβ burden. The attenuated microglia response in TREM2 cases not only affected levels of phosphorylated tau protein, but also had a profound impact on the plaque microenvironment as demonstrated by GeoMx digital spatial protein profiling.

While the Trem2 p.R47H variant described in our study has been strongly associated with increased risk for the development of AD [7, 8], it has recently also been demonstrated in the context of FTD and PD [52]. This has major mechanistic implications, since both FTD and PD are mainly characterized by intracellular protein pathology without major deposition of extracellular Aβ, except for cases with concomitant AD pathology [4] and in vitro studies have demonstrated that Trem2 variants described in association with familial forms of FTD behave differently than the R47H variant in multiple assays [19]. However, a recent study implicating TREM2-APOE signaling in the response to apoptotic neurons [18] may provide an explanation for the association of the Trem2.R47H variant with multiple neurodegenerative diseases beyond AD.

An important association has been made between APOE signaling and Trem2 function [18, 53] and it has been proposed that the presence of at least one APOE ε4 allele is necessary to promote the effect of Trem2 variants in AD, although genetic studies in larger cohorts have refuted this hypothesis [54]. We tried to balance the presence of APOE alleles in our cohort, to minimize a potential confounding effect on the observed microglia phenotype. Although our high AD group was biased towards more APOE ε4 alleles, notably only 50% of our Trem2 variant carriers were positive for at least one ε4 allele, with only one patient carrying two APOE ε4 alleles. Given the strong association of APOE and TREM2 in animal studies [18, 53], it will be important to analyze the impact of APOE genotype on Trem2-mediated effects in larger, combined patient cohorts.

Large-scale analyses of gene expression profiles provide novel mechanistic insight into many physiological and

pathological conditions, but in human disease studies, the availability of fresh-frozen tissue often limits the scale of these gene expression studies. We demonstrate here that the NanoString nCounter system is useful for the interrogation of FFPE archival tissue samples and utilized this platform to identify transcriptional differences in our cohort. Gene expression analyses revealed profound differences in multiple inflammation, neuronal, and synaptic integrity pathways as well as astrocyte associated pathways between the brain regions analyzed. Regional heterogeneity of microglia cells has been reported in the previous studies [55–59] and has been suggested to differentially affect disease progression in animal models of neurodegeneration. We demonstrate here that on a global scale, immune response patterns differ vastly from brain region to brain region within individual AD brains, most likely reflecting different stages of disease progression. These data suggest that the picture of immune response in human AD brains is very complex with multiple, brain region-specific activation patterns that may require differential therapeutic targeting.

Our studies of multiple brain regions in human AD samples also revealed profound region-specific differences between TREM2 and high AD cases. We observed an overall attenuated immune response profile in the visual cortex, which represents an area undergoing earlier stage disease processes, of TREM2 compared to high AD cases, in line with observations in TREM2-deficient animal models [13, 15, 16] and suggesting attenuating early response to pathology. In frontal cortex samples, however, representing an intermediate stage of disease progression, TREM2 cases showed exacerbated pro-inflammatory responses compared to high AD cases, consistent with a loss of the proposed functions of TREM2 in suppression of pro-inflammatory-signaling pathways in macrophages [60]. In hippocampal samples, which represent an end-stage snapshot of disease processes, the picture was mixed, with increased DAM pathways in TREM2 cases and a downregulation of astrocyte function-associated pathways. Taken together, these differences likely reflect the spreading of pathology within individual AD brains [23, 61] and represent a time course of AD progression. This sheds an important light on regional heterogeneity of pathology in human neurogenerative diseases and provides a note of caution for therapeutic development and translational studies from murine models limited to one brain region in human samples.

Acknowledgements This work was supported by a supplement to NIH/NIA P30 AG010124 (J.Q.T.) to S.P. We thank Teresa Schuck, John Robinson and Catherine Casalnova for excellent technical support.

Author contributions SP, KRM, JQT, and VYML conceived the study and co-wrote the manuscript. SP and KRM supervised and performed experiments. SN, LC, KH, SRL, and RMP performed biochemical experiments. RMP, SRL, KH, SP, and KRM performed histological experiments. SP and KRM performed gene expression analysis and Nanostring nCounter experiments. AR performed GeoMx analysis. SP and KRM performed microglia analysis. SP performed digital image analysis. SP and JQT quantified and confirmed neuropathological changes. JQT and VYML supervised the study.

Compliance with ethical standards

Conflict of interest K.R.M. and A.R. are employees of Nanostring.

References

1. Querfurth HW, LaFerla FM (2010) Alzheimer's disease. N Engl J Med 362:329–344. https://doi.org/10.1056/NEJMra0909142
2. Montine TJ, Phelps CH, Beach TG, Bigio EH, Cairns NJ, Dickson DW et al (2012) National Institute on Aging–Alzheimer's Association guidelines for the neuropathologic assessment of Alzheimer's disease: a practical approach. Acta Neuropathol 123:1–11. https://doi.org/10.1007/s00401-011-0910-3
3. Prokop S, Miller KR, Heppner FL (2013) Microglia actions in Alzheimer's disease. Acta Neuropathol 126:461–477. https://doi.org/10.1007/s00401-013-1182-x
4. Robinson JL, Lee EB, Xie SX, Rennert L, Suh E, Bredenberg C et al (2018) Neurodegenerative disease concomitant proteinopathies are prevalent, age-related and APOE4-associated. Brain 141:2181–2193. https://doi.org/10.1093/brain/awy146
5. Galatro TF, Holtman IR, Lerario AM, Vainchtein ID, Brouwer N, Sola PR et al (2017) Transcriptomic analysis of purified human cortical microglia reveals age-associated changes. Nat Neurosci 20:1162–1171. https://doi.org/10.1038/nn.4597
6. Gosselin D, Skola D, Coufal NG, Holtman IR, Schlachetzki JCM, Sajti E et al (2017) An environment-dependent transcriptional network specifies human microglia identity. Science 80-(356):eaal3222. https://doi.org/10.1126/science.aal3222
7. Guerreiro R, Wojtas A, Bras J, Carrasquillo M, Rogaeva E, Majounie E et al (2013) *TREM2* variants in Alzheimer's disease. N Engl J Med 368:117–127. https://doi.org/10.1056/NEJMoa1211851
8. Jonsson T, Stefansson H, Steinberg S, Jonsdottir I, Jonsson PV, Snaedal J et al (2013) Variant of *TREM2* associated with the risk of Alzheimer's disease. N Engl J Med 368:107–116. https://doi.org/10.1056/NEJMoa1211103
9. Sims R, van der Lee SJ, Naj AC, Bellenguez C, Badarinarayan N, Jakobsdottir J et al (2017) Rare coding variants in PLCG2, ABI3, and TREM2 implicate microglial-mediated innate immunity in Alzheimer's disease. Nat Genet 49:1373–1384. https://doi.org/10.1038/ng.3916
10. Hamza TH, Zabetian CP, Tenesa A, Laederach A, Montimurro J, Yearout D et al (2010) Common genetic variation in the HLA region is associated with late-onset sporadic Parkinson's disease. Nat Genet 42:781–785. https://doi.org/10.1038/ng.642
11. Broce I, Karch CM, Wen N, Fan CC, Wang Y, Hong Tan C et al (2018) Immune-related genetic enrichment in frontotemporal dementia: an analysis of genome-wide association studies. PLoS Med 15:e1002487. https://doi.org/10.1371/journal.pmed.1002487
12. Le Ber I, De Septenville A, Guerreiro R, Bras J, Camuzat A, Caroppo P et al (2014) Homozygous TREM2 mutation in a family with atypical frontotemporal dementia. Neurobiol Aging 35:2419.e23–2419.e25. https://doi.org/10.1016/j.neurobiolaging.2014.04.010
13. Leyns CEG, Ulrich JD, Finn MB, Stewart FR, Koscal LJ, Remolina Serrano J et al (2017) TREM2 deficiency attenuates neuroinflammation and protects against neurodegeneration in a mouse

model of tauopathy. Proc Natl Acad Sci 114:11524–11529. https://doi.org/10.1073/pnas.1710311114
14. Jay TR, Miller CM, Cheng PJ, Graham LC, Bemiller S, Broihier ML et al (2015) TREM2 deficiency eliminates TREM2^{+} inflammatory macrophages and ameliorates pathology in Alzheimer's disease mouse models. J Exp Med 212:287–295. https://doi.org/10.1084/jem.20142322
15. Ulrich JD, Finn M, Wang Y, Shen A, Mahan TE, Jiang H et al (2014) Altered microglial response to Aβ plaques in APPPS1-21 mice heterozygous for TREM2. Mol Neurodegener 9:20. https://doi.org/10.1186/1750-1326-9-20
16. Yuan P, Condello C, Keene CD, Wang Y, Bird TD, Paul SM et al (2016) TREM2 haplodeficiency in mice and humans impairs the microglia barrier function leading to decreased amyloid compaction and severe axonal dystrophy. Neuron 92:252–264. https://doi.org/10.1016/j.neuron.2016.09.016
17. Wang Y, Ulland TK, Ulrich JD, Song W, Tzaferis JA, Hole JT et al (2016) TREM2-mediated early microglial response limits diffusion and toxicity of amyloid plaques. J Exp Med 213:667–675. https://doi.org/10.1084/jem.20151948
18. Krasemann S, Madore C, Cialic R, Baufeld C, Calcagno N, El Fatimy R et al (2017) The TREM2-APOE pathway drives the transcriptional phenotype of dysfunctional microglia in neurodegenerative diseases. Immunity 47:566.e9–581.e9. https://doi.org/10.1016/j.immuni.2017.08.008
19. Kleinberger G, Yamanishi Y, Suarez-Calvet M, Czirr E, Lohmann E, Cuyvers E et al (2014) TREM2 mutations implicated in neurodegeneration impair cell surface transport and phagocytosis. Sci Transl Med 6:243ra86. https://doi.org/10.1126/scitranslmed.3009093
20. Kober DL, Alexander-Brett JM, Karch CM, Cruchaga C, Colonna M, Holtzman MJ et al (2016) Neurodegenerative disease mutations in TREM2 reveal a functional surface and distinct loss-of-function mechanisms. Elife. https://doi.org/10.7554/elife.20391
21. Song W, Hooli B, Mullin K, Jin SC, Cella M, Ulland TK et al (2017) Alzheimer's disease-associated TREM2 variants exhibit either decreased or increased ligand-dependent activation. Alzheimer's Dement 13:381–387. https://doi.org/10.1016/j.jalz.2016.07.004
22. Song WM, Joshita S, Zhou Y, Ulland TK, Gilfillan S, Colonna M (2018) Humanized TREM2 mice reveal microglia-intrinsic and -extrinsic effects of R47H polymorphism. J Exp Med 215:745–760. https://doi.org/10.1084/jem.20171529
23. Brettschneider J, Del Tredici K, Lee VM-Y, Trojanowski JQ (2015) Spreading of pathology in neurodegenerative diseases: a focus on human studies. Nat Rev Neurosci 16:109–120. https://doi.org/10.1038/nrn3887
24. Toledo JB, Van Deerlin VM, Lee EB, Suh E, Baek Y, Robinson JL et al (2014) A platform for discovery: the University of Pennsylvania Integrated Neurodegenerative Disease Biobank. Alzheimer's Dement 10:477–484
25. Guo JL, Narasimhan S, Changolkar L, He Z, Stieber A, Zhang B et al (2016) Unique pathological tau conformers from Alzheimer's brains transmit tau pathology in nontransgenic mice. J Exp Med 213:2635–2654. https://doi.org/10.1084/jem.20160833
26. Merritt CR, Ong GT, Church S, Barker K, Geiss G, Hoang M et al (2019) High multiplex, digital spatial profiling of proteins and RNA in fixed tissue using genomic detection methods. bioRxiv. https://doi.org/10.1101/559021
27. Xie SX, Baek Y, Grossman M, Arnold SE, Karlawish J, Siderowf A et al (2011) Building an integrated neurodegenerative disease database at an academic health center. Alzheimers Dement 7:e84–e93. https://doi.org/10.1016/j.jalz.2010.08.233
28. Ito D, Imai Y, Ohsawa K, Nakajima K, Fukuuchi Y, Kohsaka S (1998) Microglia-specific localisation of a novel calcium binding protein, Iba1. Brain Res Mol Brain Res 57:1–9
29. Streit WJ, Braak H, Xue Q-S, Bechmann I (2009) Dystrophic (senescent) rather than activated microglial cells are associated with tau pathology and likely precede neurodegeneration in Alzheimer's disease. Acta Neuropathol 118:475–485. https://doi.org/10.1007/s00401-009-0556-6
30. Tischer J, Krueger M, Mueller W, Staszewski O, Prinz M, Streit WJ et al (2016) Inhomogeneous distribution of Iba-1 characterizes microglial pathology in Alzheimer's disease. Glia 64:1562–1572. https://doi.org/10.1002/glia.23024
31. Thal DR, Rüb U, Orantes M, Braak H (2002) Phases of A beta-deposition in the human brain and its relevance for the development of AD. Neurology 58:1791–1800
32. Braak H, Alafuzoff I, Arzberger T, Kretzschmar H, Del Tredici K (2006) Staging of Alzheimer disease-associated neurofibrillary pathology using paraffin sections and immunocytochemistry. Acta Neuropathol 112:389–404. https://doi.org/10.1007/s00401-006-0127-z
33. Braak H, Braak E (1991) Neuropathological stageing of Alzheimer-related changes. Acta Neuropathol 82:239–259
34. Mittelbronn M, Dietz K, Schluesener HJ, Meyermann R (2001) Local distribution of microglia in the normal adult human central nervous system differs by up to one order of magnitude. Acta Neuropathol 101:249–255
35. Crary JF, Trojanowski JQ, Schneider JA, Abisambra JF, Abner EL, Alafuzoff I et al (2014) Primary age-related tauopathy (PART): a common pathology associated with human aging. Acta Neuropathol 128:755–766. https://doi.org/10.1007/s00401-014-1349-0
36. Wang J, Dickson DW, Trojanowski JQ, Lee VM-Y (1999) The levels of soluble versus insoluble brain Aβ distinguish Alzheimer's disease from normal and pathologic aging. Exp Neurol 158:328–337. https://doi.org/10.1006/exnr.1999.7085
37. Liddelow SA, Guttenplan KA, Clarke LE, Bennett FC, Bohlen CJ, Schirmer L et al (2017) Neurotoxic reactive astrocytes are induced by activated microglia. Nature 541:481–487. https://doi.org/10.1038/nature21029
38. Shi Y, Yamada K, Liddelow SA, Smith ST, Zhao L, Luo W et al (2017) ApoE4 markedly exacerbates tau-mediated neurodegeneration in a mouse model of tauopathy. Nature 549:523–527. https://doi.org/10.1038/nature24016
39. Keren-Shaul H, Spinrad A, Weiner A, Matcovitch-Natan O, Dvir-Szternfeld R, Ulland TK et al (2017) A unique microglia type associated with restricting development of Alzheimer's disease. Cell 169:1276.e17–1290.e17. https://doi.org/10.1016/j.cell.2017.05.018
40. Streit WJ, Braak H, Del Tredici K, Leyh J, Lier J, Khoshbouei H et al (2018) Microglial activation occurs late during preclinical Alzheimer's disease. Glia 66:2550–2562. https://doi.org/10.1002/glia.23510
41. De Strooper B, Karran E (2016) The cellular phase of Alzheimer's disease. Cell 164:603–615. https://doi.org/10.1016/j.cell.2015.12.056
42. Sanchez-Mejias E, Navarro V, Jimenez S, Sanchez-Mico M, Sanchez-Varo R, Nuñez-Diaz C et al (2016) Soluble phospho-tau from Alzheimer's disease hippocampus drives microglial degeneration. Acta Neuropathol 132:897–916. https://doi.org/10.1007/s00401-016-1630-5
43. Lee CYD, Daggett A, Gu X, Jiang L-L, Langfelder P, Li X et al (2018) Elevated TREM2 gene dosage reprograms microglia responsivity and ameliorates pathological phenotypes in Alzheimer's disease models. Neuron 97:1032.e5–1048.e5. https://doi.org/10.1016/j.neuron.2018.02.002
44. Li C, Zhao B, Lin C, Gong Z, An X (2018) TREM2 inhibits inflammatory responses in mouse microglia by suppressing the PI3K/NF-κB signaling. Cell Biol Int. https://doi.org/10.1002/cbin.10975

45. Linnartz-Gerlach B, Bodea L, Klaus C, Ginolhac A, Halder R, Sinkkonen L et al (2018) TREM2 triggers microglial density and age-related neuronal loss. Glia. https://doi.org/10.1002/glia.23563
46. Poliani PL, Wang Y, Fontana E, Robinette ML, Yamanishi Y, Gilfillan S et al (2015) TREM2 sustains microglial expansion during aging and response to demyelination. J Clin Invest 125:2161–2170. https://doi.org/10.1172/JCI77983
47. Ulland TK, Song WM, Huang SC-C, Ulrich JD, Sergushichev A, Beatty WL et al (2017) TREM2 maintains microglial metabolic fitness in Alzheimer's disease. Cell 170:649.e13–663.e13. https://doi.org/10.1016/j.cell.2017.07.023
48. Zheng H, Cheng B, Li Y, Li X, Chen X, Zhang Y (2018) TREM2 in Alzheimer's disease: microglial survival and energy metabolism. Front Aging Neurosci 10:395. https://doi.org/10.3389/fnagi.2018.00395
49. Bussian TJ, Aziz A, Meyer CF, Swenson BL, van Deursen JM, Baker DJ (2018) Clearance of senescent glial cells prevents tau-dependent pathology and cognitive decline. Nature 562:578–582. https://doi.org/10.1038/s41586-018-0543-y
50. Jay TR, Hirsch AM, Broihier ML, Miller CM, Neilson LE, Ransohoff RM et al (2017) Disease progression-dependent effects of TREM2 deficiency in a mouse model of Alzheimer's disease. J Neurosci 37:637–647. https://doi.org/10.1523/JNEUROSCI.2110-16.2016
51. Sayed FA, Telpoukhovskaia M, Kodama L, Li Y, Zhou Y, Le D et al (2018) Differential effects of partial and complete loss of TREM2 on microglial injury response and tauopathy. Proc Natl Acad Sci 115:10172–10177. https://doi.org/10.1073/pnas.1811411115
52. Rayaprolu S, Mullen B, Baker M, Lynch T, Finger E, Seeley WW et al (2013) TREM2 in neurodegeneration: evidence for association of the p.R47H variant with frontotemporal dementia and Parkinson's disease. Mol Neurodegener. https://doi.org/10.1186/1750-1326-8-19
53. Parhizkar S, Arzberger T, Brendel M, Kleinberger G, Deussing M, Focke C et al (2019) Loss of TREM2 function increases amyloid seeding but reduces plaque-associated ApoE. Nat Neurosci 22:191–204. https://doi.org/10.1038/s41593-018-0296-9
54. Guerreiro R, Orme T, Naj AC, Kuzma AB, Schellenberg GD, Bras J (2019) Is APOE ε4 required for Alzheimer's disease to develop in TREM2 p. R47H variant carriers? Neuropathol Appl Neurobiol 45:187–189. https://doi.org/10.1111/nan.12517
55. De Biase LM, Schuebel KE, Fusfeld ZH, Jair K, Hawes IA, Cimbro R et al (2017) Local cues establish and maintain region-specific phenotypes of basal ganglia microglia. Neuron 95:341.e6–356.e6. https://doi.org/10.1016/j.neuron.2017.06.020
56. Böttcher C, Schlickeiser S, Sneeboer MAM, Kunkel D, Knop A, Paza E et al (2019) Human microglia regional heterogeneity and phenotypes determined by multiplexed single-cell mass cytometry. Nat Neurosci 22:78–90. https://doi.org/10.1038/s41593-018-0290-2
57. Grabert K, Michoel T, Karavolos MH, Clohisey S, Baillie JK, Stevens MP et al (2016) Microglial brain region—dependent diversity and selective regional sensitivities to aging. Nat Neurosci 19:504–516. https://doi.org/10.1038/nn.4222
58. Hammond TR, Dufort C, Dissing-Olesen L, Giera S, Young A, Wysoker A et al (2019) Single-cell RNA sequencing of microglia throughout the mouse lifespan and in the injured brain reveals complex cell-state changes. Immunity 50:253.e6–271.e6. https://doi.org/10.1016/j.immuni.2018.11.004
59. Mathys H, Adaikkan C, Gao F, Young JZ, Manet E, Hemberg M et al (2017) Temporal tracking of microglia activation in neurodegeneration at single-cell resolution. Cell Rep 21:366–380. https://doi.org/10.1016/j.celrep.2017.09.039
60. Turnbull IR, Gilfillan S, Cella M, Aoshi T, Miller M, Piccio L et al (2006) Cutting edge: TREM-2 attenuates macrophage activation. J Immunol 177:3520–3524
61. Montine TJ, Monsell SE, Beach TG, Bigio EH, Bu Y, Cairns NJ et al (2016) Multisite assessment of NIA-AA guidelines for the neuropathologic evaluation of Alzheimer's disease. Alzheimer's Dement 12:164–169. https://doi.org/10.1016/j.jalz.2015.07.492